AIP Advances

Numerical investigation of multiple droplet growth dynamics on a solid surface using three-dimensional lattice Boltzmann simulations

Cite as: AIP Advances **11**, 045116 (2021); https://doi.org/10.1063/5.0045353
Submitted: 05 March 2021 • Accepted: 25 March 2021 • Published Online: 12 April 2021

Nilesh D. Pawar, Supreet Singh Bahga, Sunil R. Kale, et al.

Numerical investigation of multiple droplet growth dynamics on a solid surface using three-dimensional lattice Boltzmann simulations

Cite as: AIP Advances 11, 045116 (2021); doi: 10.1063/5.0045353
Submitted: 5 March 2021 • Accepted: 25 March 2021 •
Published Online: 12 April 2021

Nilesh D. Pawar,[1] Supreet Singh Bahga,[2] Sunil R. Kale,[2] and Sasidhar Kondaraju[3,a)]

AFFILIATIONS

[1] Department of Mechanical Engineering, BITS Pilani, K K Birla Goa Campus, Zuarinagar, Goa 403726, India
[2] Department of Mechanical Engineering, Indian Institute of Technology Delhi, Hauz Khas, New Delhi 110016, India
[3] School of Mechanical Sciences, Indian Institute of Technology Bhubaneswar, Argul, Odisha 752050, India

[a)] **Author to whom correspondence should be addressed:** sasidhar@iitbbs.ac.in

ABSTRACT

We present an investigation of multiple droplet growth dynamics on homogeneous and patterned surfaces during dropwise condensation. Our analysis is based on three-dimensional thermal lattice Boltzmann simulations. First, we investigate the growth dynamics on homogeneous surfaces. The analysis of growth dynamics of droplets on a homogeneous surface shows that the lower the static contact angle of the surface, the higher the condensed volume of liquid. After that, we discuss the growth dynamics of droplets on patterned surfaces (a surface with hydrophilic and hydrophobic regions). We show that the pattern formed by the condensed droplets on the patterned surfaces is completely different from the homogeneous surface. This is due to the pinning effect at the interface of the hydrophilic–hydrophobic region. Moreover, the shape of the droplets is not spherical, as we observe in the case of homogeneous surfaces. We also demonstrate that the condensed volume V for all patterned surfaces is higher than that for the homogeneous surface. However, the condensed volume decreases with an increase in the contact angle of the hydrophilic region. We then present the effect of size of the hydrophilic spot. We find that the condensed volume increases with an increase in radius of the hydrophilic spot.

I. INTRODUCTION

Condensation of vapor on cold surfaces, for example, drop formation on the window pane or the lid of a coffee cup, is a commonly observed phase transition phenomenon. It has garnered the interest of researchers due to its importance in the thermal technology such as power generation,[1] desalination,[2] cooling of nuclear reactors,[3] and fog water harvesting.[4] Condensation can be categorized as either filmwise condensation (FWC) or dropwise condensation (DWC). The DWC provides one order of magnitude higher heat transfer coefficients than the FWC due to periodical removal of droplets from the surface (known as the droplet shedding effect).[5] Therefore, to design surfaces that can sustain dropwise condensation, a fundamental understanding of droplet growth dynamics is imperative. Consequently, droplet growth dynamics have been a topic of research for several decades.

The pattern formed by the condensed droplets on the surface is commonly known as breath figures (BFs). Several studies have been performed to understand the droplet growth pattern and their scaling laws during breath figure formation, beginning with the work of Beysens and Knobler.[6] They identified different growth regimes on non-wetting surfaces and described them in two stages. In the initial stage, the droplets grow as an individual droplet ($R \sim t^{\mu}$). In the coalescence dominated regime, droplets mainly grow due to coalescence ($R \sim t^{\mu_0}$). Here, R denotes the average droplet radius and μ and μ_0 represent the power law exponents. Since then, the droplet growth pattern has been studied extensively to find the exponents μ and μ_0, and the transition of exponent from μ to μ_0.[7,8] All these studies employed the Monte Carlo technique due to its simplicity. In this method, droplet nucleation, growth, coalescence, and departure from the surface are considered idealized processes. The simulations begin with randomly placing droplets on the surfaces. Then, these droplets grow as an individual droplet following the power law

$R \sim t^{\mu}$, and as the two neighboring droplets touch, they are merged to form a larger droplet. The larger droplet is placed at the center of mass of the two coalescing droplets. A detailed review of these simulations can be found in a recent review article by Singh *et al.*[9] These simulations give the statistical behavior of a large number of droplets rather than the detailed information about different processes such as single droplet growth or the coalescence of droplets, and so on.

Previous studies on dropwise condensation, including those mentioned above, focused on studying the droplet growth behavior on hydrophobic surfaces. However, the energy barrier ΔG for droplet nucleation depends on the static contact angle θ of the surface given by[10]

$$\Delta G = \pi \sigma_{lv} r^{*2} (2 - 3\cos\theta + \cos^3\theta)/3. \quad (1)$$

Here, σ_{lv} and r^{*2} denote the surface tension of the liquid–vapor interface and the critical radius of a droplet, respectively. The energy barrier ΔG is zero for $\theta = 0^{\circ}$ and increases with θ and becomes maximum for $\theta = 180^{\circ}$. Therefore, the droplet preferentially nucleates on the hydrophilic surface. In several physical processes, the use of nature-inspired hybrid surfaces (a surface with hydrophilic spots on the hydrophobic surface) has been investigated.[11–13] This is due to preferential nucleation of droplets on the hydrophilic region and easy removal of droplets on the hydrophobic region. On such surfaces, the droplet growth pattern should differ from that of the homogeneous surfaces due to pinning effect at the interface of the hydrophilic–hydrophobic region. Therefore, it is crucial to study the growth pattern on hybrid surfaces. Understanding the droplet growth on patterned surfaces can be useful to design surfaces that can sustain dropwise condensation. However, the Monte Carlo method is not suitable for the hybrid surfaces due to its inability to mimic the pinning effect. In addition to the Monte Carlo method, the following techniques are commonly used to study DWC.

(i) **Molecular dynamics (MD) simulations**: In MD simulations, we consider each molecule or particle moving randomly. Therefore, by applying Newton's second law of motion, we can obtain each molecule's position and velocity. By incorporating the proper form of interaction forces between the particles and implementing the boundary conditions, DWC can be simulated without specifying any numerical artifacts.[14] MD simulations are very promising to understand the fundamental physics of DWC. However, the MD simulations are highly time-consuming and computationally expensive. Moreover, the simulations of DWC are limited to very small sizes.

(ii) **Navier–Stokes solver**: In this approach, we solve the conservation of mass, momentum, and energy equations in liquid and vapor phases, respectively.[15,16] The new terms are added to consider the effect of surface tension force and the phase change heat transfer. Furthermore, to track the liquid–vapor interface, an additional scheme such as the volume of fluid (VoF) or level set method (LSM) is usually employed. However, these techniques significantly increase the computational cost.

(iii) **Lattice Boltzmann method (LBM)**: The LBM is an effective technique for multiphase flows compared to Navier–Strokes simulations. In this approach, we do not require to track the interface as it inherently captures the interface due to inter-particle interaction forces between the fluid particles. The static contact angle is also employed via a parameter in the interaction force between fluid and solid particles. As a result, the dynamic contact angle evolves during simulations. These characteristics make the LBM appropriate to simulate multiphase flows and phase change heat transfer.

In the last three decades, the lattice Boltzmann method (LBM) has become a powerful numerical technique to simulate multiphase flows[17–19] and phase change heat transfer.[20] Several lattice Boltzmann (LB) models are available to simulate the multiphase flows.[21–23] However, the pseudopotential model proposed by Shan and Chen[22,24] is commonly used due to its simplicity. The pseudopotential model's idea is to include the non-local interaction forces between the fluid particles and between the fluid and solid particles. As a result, phase separation and the interface formation emerge naturally without employing any technique to track the interface. However, the model was limited to the isothermal flows only. Later, the model was extended to simulate the phase change heat transfer by including an energy equation solver.[25] The energy equation is solved using two ways, either by using another distribution function for temperature[26] or by using a finite difference method.[27] Hence, we have implemented the LBM to investigate the growth dynamics of droplets on a solid surface during condensation. In this work, we use two distribution functions, namely, density and temperature. These distribution functions are coupled via an equation of state on a macroscopic level.

Hazi and Markus[28] proposed a pseudopotential thermal LB model to simulate phase change heat transfer. They used two distribution functions for density and temperature fields. However, they did not employ the equation of a state of a real gas. Later, Gong and Cheng[29] extended the thermal LB model to include a real equation state. They also derived a source term that accounts for the phase change heat transfer. Subsequently, the model was extensively used to study dropwise condensation on a plane and rough structured surfaces.[30] Li *et al.*[31] studied the droplet nucleation position and the wetting state of a resulting droplet on the structured surfaces. Later, Haghani-Hassan-Abadi and Rahimian[32] investigated the DWC on impregnated surfaces. Recently, Pawar *et al.*[33] studied the growth dynamics of a single droplet on homogeneous and patterned surfaces. They explained the growth mechanisms of a droplet on the patterned surfaces. All the previous studies, including those mentioned above, are concentrated on a growth dynamics of a single droplet or the coalescence of two droplets. However, to the best of our knowledge, we know of no numerical detailed study focusing on growth dynamics of multiple droplets, in particular the pattern formed by the droplets and the coalescence process on the patterned surfaces.

To this end, we present a droplet growth dynamics on homogeneous hydrophobic and patterned surfaces using three-dimensional thermal lattice Boltzmann simulation. In particular, we show the effect of surface wettability. We then present the droplet growth pattern on hybrid surfaces. Moreover, the effect of contact angle of the hydrophilic region on the growth dynamics of hybrid surfaces. We begin by reviewing the thermal lattice Boltzmann model. We

then present the results of droplet growth pattern, followed by the conclusions.

II. NUMERICAL METHOD

In this section, we present the thermal lattice Boltzmann method for multiphase phase change heat transfer. The numerical model consists of a flow solver and the energy equation solver. We use two distribution functions for the flow solver and the energy equation solver. We begin with the flow solver followed by the energy equation solver.

A. Flow solver

The temporal evolution of the particle distribution function with the Bhatnagar–Gross–Krook (BGK)[34] collision operator is given as

$$f_i(\mathbf{x}+\mathbf{e}_i\delta t, t+\delta t) - f_i(\mathbf{x},t) = \frac{-1}{\tau}\left[f_i(\mathbf{x},t) - f_i^{eq}(\mathbf{x},t)\right] + \Delta f_i(\mathbf{x},t), \tag{2}$$

where $f_i(\mathbf{x},t)$ is the particle distribution function in the ith direction with discrete particle velocity $\mathbf{e}_i$ at location $\mathbf{x}$ and time t. τ is the dimensionless relaxation time, and f_i^{eq} is the corresponding equilibrium distribution function, which is given by Yu *et al.*[35]

$$f_i^{eq} = \rho w_i\left[1 + 3\frac{(\mathbf{e}_i\cdot\mathbf{u})}{c^2} + \frac{9}{2}\frac{(\mathbf{e}_i\cdot\mathbf{u})^2}{c^4} - \frac{3}{2}\frac{\mathbf{u}^2}{c^2}\right], \tag{3}$$

where $c = \delta x/\delta t$ is the lattice speed, δx and δt are the lattice spacing and time step, respectively, and w_i is the weighting factor. We use three-dimensional lattice arrangement with 19 discrete velocities (D3Q19), as shown in Fig. 1. The weighting factor w_i and discrete particle velocities for the D3Q19 model are given as

$$w_i = \begin{cases} 1/3, & i = 0 \\ 1/18, & i = 1,2,\ldots,6 \\ 1/36, & i = 5,6,\ldots,18, \end{cases} \tag{4}$$

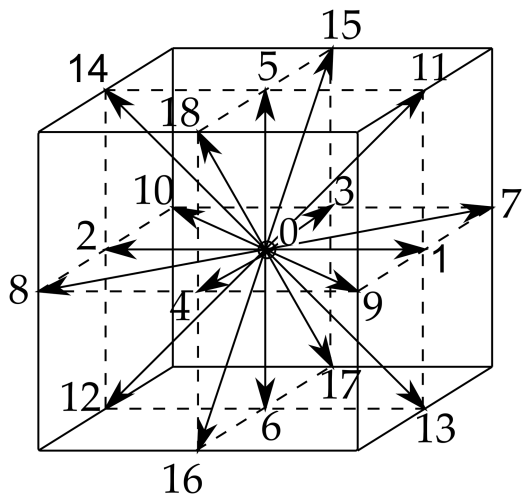

FIG. 1. Three-dimensional lattice arrangement with 19 discreet velocities (D3Q19).

$$\mathbf{e}_i = \begin{cases} (0,0,0), & i = 0 \\ (\pm1,0,0)c, (0,\pm1,0)c, (0,0,\pm1)c, & i = 1,2,\ldots,6 \\ (\pm1,\pm1,0)c, (\pm1,0,\pm1)c, (0,\pm1,\pm1)c, & i = 5,6,\ldots,18. \end{cases} \tag{5}$$

Equation (2) is solved in the following two steps:

1. Collision:
   The particles arriving at a node collide and change their direction. The post-collision distribution functions are calculated as

$$f_i^*(\mathbf{x},t) = f_i(\mathbf{x},t) - \frac{1}{\tau}\left[f_i(\mathbf{x},t) - f_i^{eq}(\mathbf{x},t)\right]. \tag{6}$$

2. Streaming:
   The particles move to the neighboring node corresponding to their velocity directions,

$$f_i(\mathbf{x}+\mathbf{e}_i\delta t, t+\delta t) = f_i^*(\mathbf{x},t). \tag{7}$$

To implement the body force term $\Delta f_i(\mathbf{x},t)$, we used the exact difference method (EDM) proposed by Kupershtokh,[36,37]

$$\Delta f_i(\mathbf{x},t) = f_i^{eq}(\rho(\mathbf{x},t), \mathbf{u}+\Delta\mathbf{u}) - f_i^{eq}(\rho(\mathbf{x},t),\mathbf{u}), \tag{8}$$

where $\Delta\mathbf{u} = \mathbf{F}\delta t/\rho$ is the velocity change due to the action of total force $\mathbf{F}$ during the time step Δt. The macroscopic density ρ and velocity $\mathbf{u}$ are calculated as

$$\rho = \sum_{i=0}^{b} f_i = \sum_{i=0}^{b} f_i^{eq}, \tag{9}$$

$$\rho\mathbf{u} = \sum_{i=0}^{b} f_i\mathbf{e}_i + \frac{\delta t}{2}\mathbf{F} = \sum_{i=0}^{b} f_i^{eq}\mathbf{e}_i + \frac{\delta t}{2}\mathbf{F}. \tag{10}$$

The kinematic viscosity ν is calculated using relaxation time τ by

$$\nu = c_s^2\left(\tau - \frac{1}{2}\right)\delta t, \tag{11}$$

where c_s is the speed of sound and is given as $c_s = c/\sqrt{3}$.

The fluid particles (or pseudoparticles) reside on every lattice site. These particles interact via interaction forces. Therefore, we consider two types of interaction forces between the fluid and fluid particles and between the fluid and the solid particles (or solid wall). Shan and Chen[22,24] introduced pseudopotential ψ to simulate nonlocal interactions between the fluid particles. For single-component multiphase flow, the interaction force acting on the particles at site $\mathbf{x}$ is given by

$$\mathbf{F}_{\text{int}}(\mathbf{x}) = -G\psi(\mathbf{x})\sum_i w_i\psi(\mathbf{x}+\mathbf{e}_i\delta t)\mathbf{e}_i, \tag{12}$$

where G is a parameter that controls the strength of the interaction force. The pseudopotential function ψ is given as[38]

$$\psi(\mathbf{x}) = \sqrt{\frac{2(p-\rho c_s^2)}{Gc_s^2}}, \tag{13}$$

where p is the pressure, and we used $G = -1$ in this study. The pressure p is calculated using the Peng–Robinson (P–R) equation of state as follows:[38]

$$p = \frac{\rho RT}{1 - b\rho} - \frac{a\rho^2\,\varepsilon(T)}{1 + 2b\rho - b^2\rho^2}, \tag{14}$$

$$\varepsilon(T) = \left[1 + (0.374\,64 + 1.542\,26\omega - 0.269\,92\omega^2)\left(1 - \sqrt{\frac{T}{T_c}}\right)\right]^2, \tag{15}$$

where $a = 0.5472R^2T_c^2/p_c$ and $b = 0.0778RT/p_c$. In this work, we used $R = 1, a = 2/49$, and $b = 2/21$. In addition, the interaction force between the fluid and the solid wall is given as

$$\mathbf{F}_{\text{ads}}(\mathbf{x}) = -G_{\text{ads}}\psi(\mathbf{x})\sum_i w_i s(\mathbf{x} + \mathbf{e}_i\delta t)\mathbf{e}_i. \tag{16}$$

The parameter G_{ads} controls the strength of the interaction force between the fluid and the solid wall. The different contact angles are obtained by adjusting G_{ads} values, and $s(\mathbf{x} + \mathbf{e}_i\delta t)$ is an indicator function, which is expressed as

$$s(\mathbf{x} + \mathbf{x}\delta t) = \begin{cases} 0 & \text{if } (\mathbf{x} + \mathbf{e}_i\delta t) \text{ is fluid node} \\ 1 & \text{if } (\mathbf{x} + \mathbf{e}_i\delta t) \text{ is solid node.} \end{cases}$$

Therefore, the total force acting at each site $\mathbf{x}$ is given by

$$\mathbf{F} = \mathbf{F}_{\text{int}} + \mathbf{F}_{\text{ads}}. \tag{17}$$

B. Energy equation solver

We begin with the conservation of energy equation as follows:[27]

$$\frac{\partial T}{\partial t} + \nabla\cdot(\mathbf{u}T) = \frac{1}{\rho c_v}\nabla\cdot(k\nabla T) + T\left[1 - \frac{1}{\rho c_v}\left(\frac{\partial p}{\partial T}\right)_\rho\right]\nabla\cdot\mathbf{u}. \tag{18}$$

Here T, k, and c_v denote the temperature, thermal conductivity, and specific heat at constant volume, respectively. The above equation can also be written as

$$\underline{\frac{\partial T}{\partial t} + \nabla\cdot(\mathbf{u}T) = \nabla\cdot(\alpha\nabla T)} + \phi, \tag{19}$$

where α and ϕ denote the thermal diffusivity and the source term that accounts for the phase change heat transfer, respectively. The source term ϕ is given as

$$\phi = \left[\frac{1}{\rho c_v}\nabla\cdot(k\nabla T) - \nabla\cdot(\alpha\nabla T)\right] + T\left[1 - \frac{1}{\rho c_v}\left(\frac{\partial p}{\partial T}\right)_\rho\right]\nabla\cdot\mathbf{u}. \tag{20}$$

Equation (19) is the target transport equation that we intend to solve to model the phase change heat transfer. The underlined terms in Eq. (19) are solved using the thermal LB equation. Therefore, we use an additional distribution function for the temperature field. Furthermore, we calculate the source term ϕ using a finite difference scheme and then add into thermal LBE. The thermal LBE is given by Gong and Cheng as

$$\mathrm{g}_i(\mathbf{x} + \mathbf{e}_i\delta t, t + \delta t) - \mathrm{g}_i(\mathbf{x}, t) = \frac{-1}{\tau_{\mathrm{g}}}\left[\mathrm{g}_i(\mathbf{x}, t) - \mathrm{g}_i^{eq}(\mathbf{x}, t)\right] + \delta t\, w_i\phi, \tag{21}$$

where $\mathrm{g}_i(\mathbf{x}, t)$ is the temperature distribution function along the ith direction, τ_{g} is the dimensionless relaxation time for temperature, and $\mathrm{g}_i^{eq}(\mathbf{x}, t)$ is its corresponding equilibrium temperature distribution and is expressed as

$$\mathrm{g}_i^{eq}(\mathbf{x}, t) = Tw_i\left[1 + \frac{\mathbf{e}_i\cdot\mathbf{u}}{c_s^2} + \frac{(\mathbf{e}_i\cdot\mathbf{u})^2}{2c_s^4} - \frac{\mathbf{u}^2}{2c_s^2}\right]. \tag{22}$$

The macroscopic temperature T is calculated from the temperature distribution function by

$$T = \sum_i \mathrm{g}_i. \tag{23}$$

The thermal diffusivity α is calculated using the relaxation time of temperature τ_{g} by

$$\alpha = c_s^2\left(\tau_{\mathrm{g}} - \frac{1}{2}\right)\delta t. \tag{24}$$

Different viscosity ratios can be achieved by expressing the relaxation time as a linear function of local fluid density,[39,40]

$$\tau(\rho) = \frac{(\tau_l - \tau_v)}{(\rho_l - \rho_v)}\rho + \frac{(\tau_v\rho_l - \tau_l\rho_v)}{(\rho_l - \rho_v)}, \tag{25}$$

where τ_l and τ_v are the relaxation times corresponding to coexistence densities of liquid and vapor phases. Different thermal diffusivity ratios can be obtained similarly.

III. SIMULATION DETAILS

In this section, we provide the simulation details. We performed simulation on homogeneous and patterned surfaces.

A. Homogeneous surfaces

Schematic of the computational domain is shown in Fig. 2. We performed three-dimensional simulations in a domain of size $300 \times 300 \times 400$ lattice units. We employed a half-way bounce-back scheme at $z = 0$ and $z = Nz$ and the periodic condition in the $x-$ and y-direction. Initially, the domain was occupied by vapor at saturation temperature $T_s = 0.9T_{\text{cr}}$. The corresponding coexistence properties of the liquid and vapor can be found in Refs. 33 and 41. We created 80 cold circular spots of radius 12.5 μm each randomly by fixing the wall temperature to $T_w = 0.75T_{\text{cr}}$ at the bottom wall, which acts as nucleation sites. The rest of the wall was at Ts. As the drop grows, we extend the cold spot size to the size of droplet base diameter to ensure that the temperature underneath the drop is $T_w = 0.75T_{\text{cr}}$.

While creating the random nucleation sites, we maintained a minimum distance of $1.2R$ between two neighboring sites, where R is the droplet radius. For homogeneous surfaces, our objective is to study the effect of surface wettability on droplet growth dynamics. The surface wettability is characterized in terms of contact angle θ. We obtain different contact angles by changing the parameter G_{ads} in Eq. (16). In this work, we present the results for contact angles of 90°, 120°, and 150°. We compare the performance of different surfaces in terms of condensed volume V and surface coverage ε^2.

B. Patterned surfaces

The computational domain and boundary conditions are the same as in Sec. III A. We periodically arranged 81 hydrophilic circular spots of radius 12.5 μm each on the hydrophobic sur-

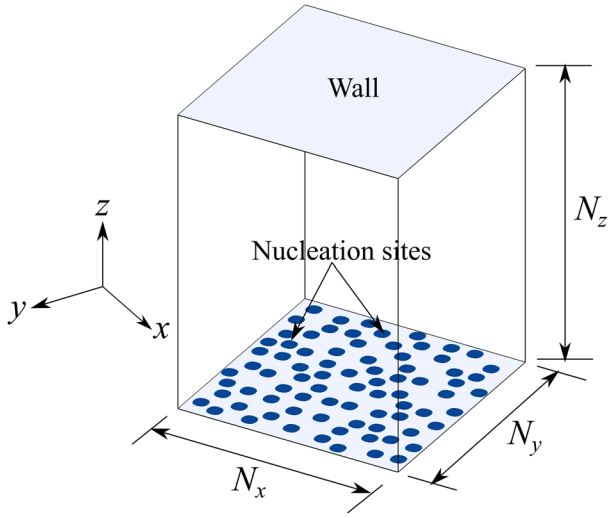

FIG. 2. Schematic of the computational domain for the homogeneous surface. We employed the half-way bounce-back condition at $z = 0$ and $z = Nz$, and the periodic condition in the $x-$ and y-direction. Initially, the domain was occupied by vapor at saturation temperature $T_s = 0.9T_{cr}$. We created 80 cold circular spots of radius 12.5 μm each by fixing the wall temperature to $T_w = 0.75T_{cr}$ at the bottom wall, which act as nucleation sites.

face, as shown in Fig. 3. The distance between two hydrophilic spots is 37.5 μm in the x- and y-direction. To create hydrophilic spots on the surfaces, we changed G_{ads} in Eq. (16) in the circular region such that we achieve a hydrophilic surface. For the rest of the surface, we choose G_{ads} to obtain the hydrophobic surface. The distance between two circular spots is

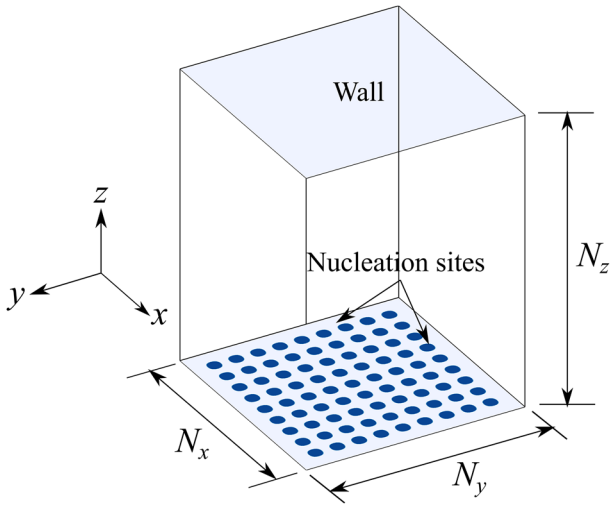

FIG. 3. Schematic of the computational domain for the patterned surface. We periodically arranged 81 hydrophilic circular spots of radius 12.5 μm each on the hydrophobic surface. The distance between two circular spots is 37.5 μm. We kept the whole surface at the same temperature $T_w = 0.82T_{cr}$.

37.5 μm. We kept the whole surface at the same temperature of $T_w = 0.82T_{cr}$.

For patterned surfaces, our objective is to study the effect of hydrophilic patches on a hydrophobic surface. We study different patterned surfaces by varying the contact angle of the hydrophilic spots for the same hydrophobic surface. In this work, we consider hydrophilic spots with contact angles of 30°, 50°, 70°, and 90°. We compare the performance of different patterned surfaces in terms of condensed volume V and surface coverage ε^2. Moreover, we also show the effect of size of the hydrophilic spot on condensed volume V.

IV. RESULTS AND DISCUSSION

In this section, we present results obtained from the thermal LBM simulations. We have shown a detailed validation of our code in our previous papers.[33,41] We begin with the results of droplet growth on homogeneous surfaces followed by growth dynamics on patterned surfaces.

A. Growth dynamics on homogeneous hydrophobic surfaces

To study the effect of surface wettability, we varied the contact angles of the surface. We compare the performance of different surfaces in terms of the condensed volume of liquid V and the surface coverage ε^2. We performed simulations for $\theta = 90°$, 120°, and 150°. Figure 4 shows the temporal evolution of droplets on surfaces with varying wettability. We find that droplets nucleate at random nucleation sites on the surface. First, we observe that droplets nucleate quickly on a surface with lower wettability. The time when we observe droplets first increases with the contact angle of the surface θ. This is in agreement with the experimental results.[42] Next, the droplets grow with time due to direct condensation at the liquid–vapor interface of droplets. However, droplets are separated from each other and grow as an individual drop. As the condensation continues, the distance between the droplet decreases with time, and droplets start coalescing with neighboring droplets. Therefore, droplets grow because of two mechanisms: (i) direct condensation at the liquid–vapor interface and (ii) coalescence with neighboring droplets. In the end, there are only a few droplets apart from each other and grow due to direct condensation.

Figure 5(a) shows the condensed volume of liquid as a function of time for three different surfaces with contact angles of 90°, 120°, and 150°. Initially, we find that the lower the static contact angle of the surface, the higher the condensed volume of liquid. The higher amount of condensed liquid on a surface with a lower contact angle is attributed to the higher solid–liquid contact area and lower conduction resistance. As time increases, the droplets coalesce with neighboring droplets and form larger droplets. This results in increased conduction resistance and lower liquid–vapor interfacial area. Therefore, the growth rate of droplets reduces with time and, hence, the condensed volume of liquid saturates at later times. We also observe that at the final stage of condensation, the condensed volume for $\theta = 150°$ approaches that for the lower contact angle 90°. This is because the surface with a contact angle of

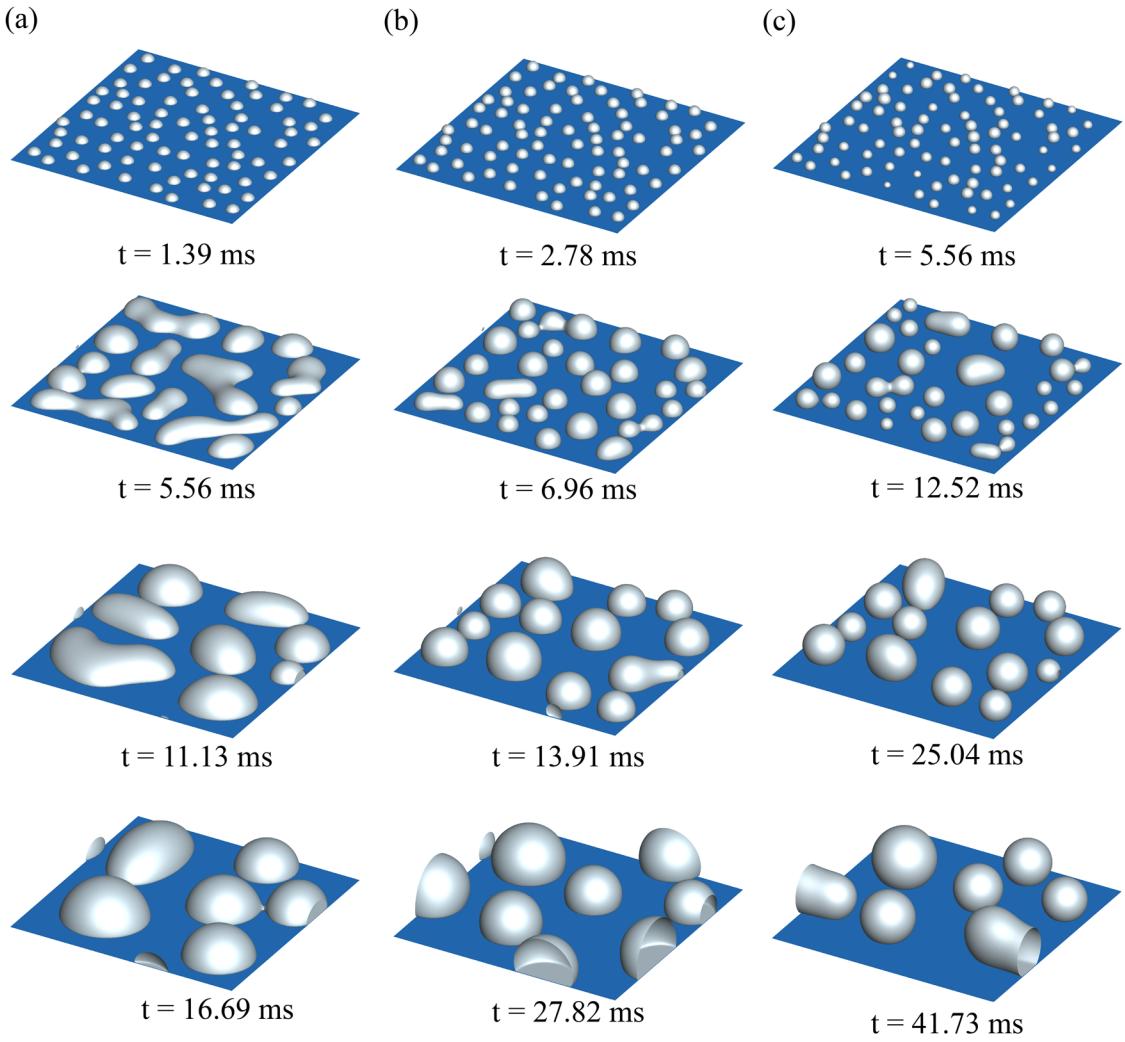

FIG. 4. Temporal evolution of droplets on a surface with different contact angles. (a) $\theta = 90°$. (b) $\theta = 120°$. (c) $\theta = 150°$.

150° has more number of droplets than the surface with a contact angle of 90°, which results in more liquid–vapor interfacial area.

Figure 5(b) shows the evolution of surface coverage ε^2 with time t for different wettability surfaces. Initially, surface coverage increases with time because the droplets grow as an individual droplet. As the coverage reaches a maximum value, the droplets start coalescing with neighboring droplets. Therefore, the surface coverage decreases with time on a surface with $\theta = 90°$. However, the coverage remains approximately constant on the hydrophobic surfaces. This is because the droplet growth is balanced by the direct condensation and the coalescence events. The maximum coverage decreases with an increase in contact angle of the surface. The surface coverage shows the maximum value of 0.57, 0.35, and 0.14 for surfaces with contact angle of 90°, 120°, and 150°, respectively.

B. Growth dynamics on patterned surfaces

In this section, we discuss the results of the growth dynamics of droplets on patterned surfaces (a surface with hydrophilic and hydrophobic regions).

Figure 6 shows the droplet growth pattern on a patterned surface with contact angles of hydrophilic and hydrophobic regions being 30° and 150°, respectively. Due to the lower energy barrier, droplets preferentially nucleate on the hydrophilic spots and form wet spots on the surface. When the contact line comes in contact with a local chemical or geometrical defect, the droplet cannot move even when capillary force is applied to it. This phenomenon is known as pinning. The interface of the hydrophilic surface and the hydrophobic surface acts as chemical defects, and the contact line pins there. Because of contact line pinning at the interface of the hydrophilic–hydrophobic region, droplets grow in the CCL

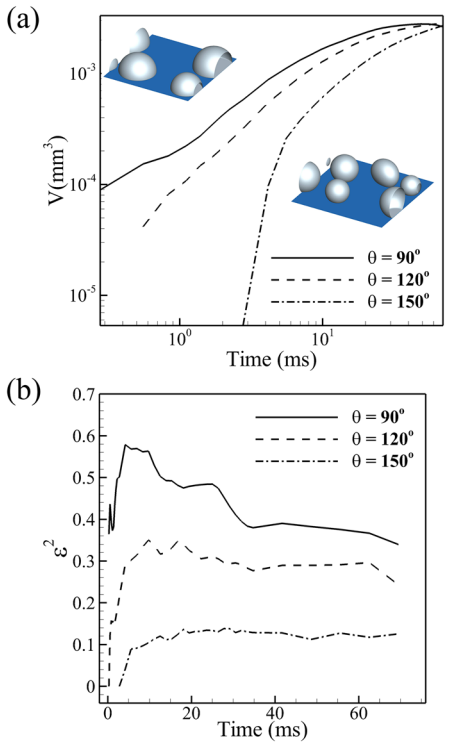

FIG. 5. Growth dynamics of droplets on different wettability surfaces. (a) Variation of total condensed volume V of liquid with time t. (b) Evolution of surface coverage ε^2 with time t.

growth mode. When the neighboring droplets touch, they coalesce to form large droplets. However, the shape of the droplets is not spherical as we observed in the case of homogeneous surfaces in Sec. III A. This irregular shape of droplets is caused by the contact line pinning effect. Moreover, the pattern formed by the droplets is completely different than the homogeneous surface. Due to the periodic arrangement of the hydrophilic region, controlled coalescence of droplets occurs. We also observe the re-nucleation of droplets on the hydrophilic region, as shown in Fig. 6(e). Then, these re-nucleated droplets get absorbed by the larger droplets, as shown in Fig. 6(f).

Figure 7 shows the volume of condensed liquid V and the surface coverage ε^2 with time t for four different patterned surfaces. Here, we define the surface coverage as the ratio of area covered by the droplets to the total surface area. We also showed results of the homogeneous surface with $\theta = 150^\circ$ for comparison. Henceforth, the patterned surfaces will be represented as θ_1–θ_2, where θ_1 and θ_2 denote the contact angle of the hydrophilic and hydrophobic region, respectively. In the initial period, we observed that the patterned surface 30°–150° has the highest condensed volume V, as shown in Fig. 7(a). However, the condensed volume V decreases with an increase in θ_1. As time increases, large droplets form due to coalescence events and the growth of droplet slows down. However, the condensed volume of liquid V for all patterned surfaces is higher than the homogeneous surface with $\theta = 150^\circ$. Figure 7(b) shows the time evolution of surface coverage ε^2 for different patterned surfaces. We observed that the maximum surface coverage decreases with an increase in θ_1. However, the homogeneous surface has the lowest surface coverage.

We further analyzed the effect of size of the hydrophilic spot on droplet growth. We have performed simulations on three different types of patterned surfaces with the radii of the hydrophilic region being 10, 12.5, and 15 μm. Figure 8 shows the condensed volume of liquid V with time t for different patterned surfaces. We observe that the condensed volume of liquid increases with an increase in the radius of the hydrophilic spot. This is expected because as the radius of the hydrophilic spot increases, a larger wet spot forms on the surface. Therefore, a larger solid–liquid contact area results in higher condensed volume.

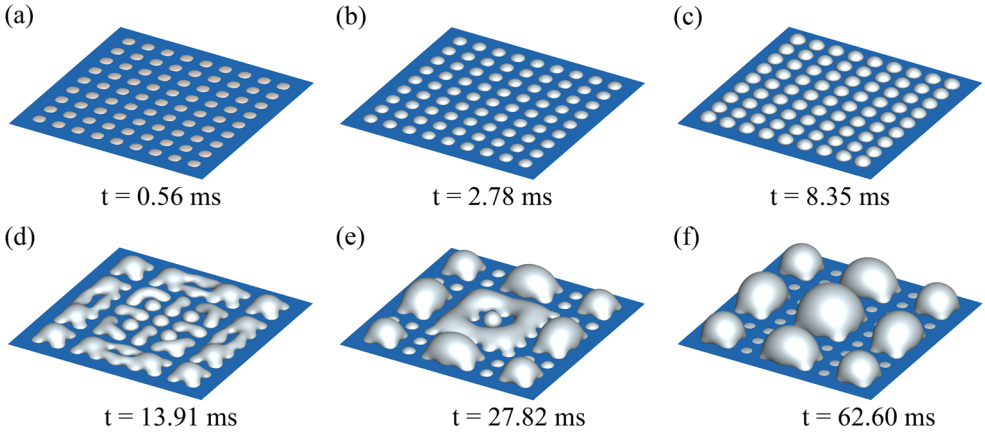

FIG. 6. Growth dynamics of droplets on a patterned surface as a function of time. The contact angle of the hydrophilic region and the hydrophobic region is 30° and 150°, respectively. (a) Start of visible condensation on hydrophilic spots at t = 0.56 ms, (b) growth of droplets on hydrophilic spots at t = 2.78 ms, (c) the droplets grow to a contact angle of 30° at t = 8.35 ms, which is the equilibrium contact angle for the hydrophilic spots, (d) the growth coupled with coalescence of multiple droplets can be observed at t = 13.91 ms, (e) the coalescence on hybrid surfaces at t = 27.82 ms shows some of the hydrophilic spots cleared during the coalescence of multiple droplets, and (f) the coalescence at t = 62.60 ms shows a strong pinning of the droplets at the interface of hydrophilic spots and hydrophobic surfaces. The droplets' contact angle during the coalescence increases from 30° to 150°.

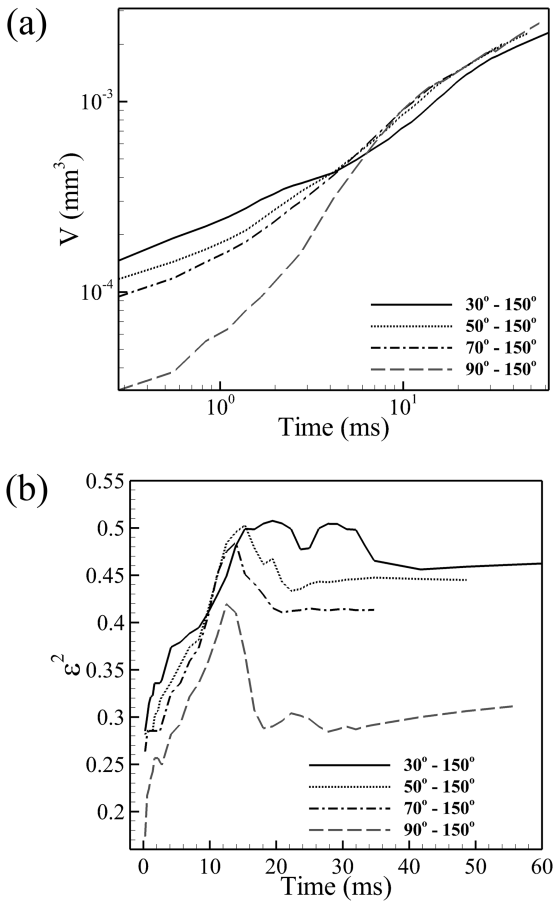

FIG. 7. Growth dynamics of droplets on four different patterned surfaces. (a) Variation of the total condensed volume of liquid V with time t. (b) Evolution of surface coverage ε^2 with time t.

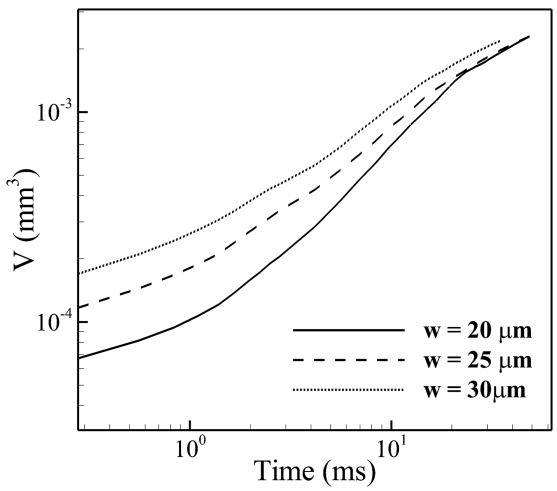

FIG. 8. Effect of the size of the hydrophilic spot on the evolution of condensed volume V with time t.

V. CONCLUSION

We have investigated the droplet growth dynamics on homogeneous and patterned surfaces using three-dimensional lattice Boltzmann simulations. Initially, we performed simulations on homogeneous surfaces. We observed that the lower the static contact angle of the surface, the higher the condensed volume of liquid. After that, we analyzed the droplet growth dynamics on patterned surfaces. We found that the pattern formed by the condensed droplets on the patterned surface is completely different from the homogeneous surface. This is due to the pinning effect at the interface of the hydrophilic–hydrophobic regions. Moreover, the shape of the droplet is not spherical as we observed in the case of homogeneous surfaces. We also studied the effect of the contact angle of the hydrophilic region θ_1 of the patterned surfaces. We observed that the condensed volume decreases with an increase in θ_1. We also showed that the condensed volume V for all patterned surfaces is higher than that for the homogeneous surface. Finally, we have also explored the effect of the size of the hydrophilic spot. We found that the condensed volume increases with an increase in hydrophilic spot size.

ACKNOWLEDGMENTS

The authors thank IIT Delhi HPC for providing the supercomputing facility and the Department of Science and Technology, Government of India, via Grant No. IMP/2018/000422 for providing support for this research.

DATA AVAILABILITY

The data that support the findings of this study are available from the corresponding author upon reasonable request.

REFERENCES

[1] J. M. Beér, "High efficiency electric power generation: The environmental role," Prog. Energy Combust. Sci. **33**, 107–134 (2007).
[2] A. D. Khawaji, I. K. Kutubkhanah, and J.-M. Wie, "Advances in seawater desalination technologies," Desalination **221**, 47–69 (2008).
[3] M. H. Kim and M. L. Corradini, "Modeling of condensation heat transfer in a reactor containment," Nucl. Eng. Des. **118**, 193–212 (1990).
[4] A. Lee, M.-W. Moon, H. Lim, W.-D. Kim, and H.-Y. Kim, "Water harvest via dewing," Langmuir **28**, 10183–10191 (2012).
[5] V. P. Carey, *Liquid Vapor Phase Change Phenomena: An Introduction to the Thermophysics of Vaporization and Condensation Process in Heat Transfer Equipment* (Taylor & Francis, 2007).
[6] D. Beysens and C. M. Knobler, "Growth of breath figures," Phys. Rev. Lett. **57**, 1433–1436 (1986).
[7] J. L. Viovy, D. Beysens, and C. M. Knobler, "Scaling description for the growth of condensation patterns on surfaces," Phys. Rev. A **37**, 4965–4970 (1988).
[8] D. Fritter, C. M. Knobler, D. Roux, and D. Beysens, "Computer simulations of the growth of breath figures," J. Stat. Phys. **52**, 1447–1459 (1988).
[9] M. Singh, N. D. Pawar, S. Kondaraju, and S. S. Bahga, "Modeling and simulation of dropwise condensation: A review," J. Indian Inst. Sci. **99**, 157–171 (2019).
[10] K. Kelton and A. L. Greer, *Nucleation in Condensed Matter: Applications in Materials and Biology* (Elsevier, 2010).
[11] A. Ghosh, S. Beaini, B. J. Zhang, R. Ganguly, and C. M. Megaridis, "Enhancing dropwise condensation through bioinspired wettability patterning," Langmuir **30**, 13103–13115 (2014).

[12]B. Mondal, M. Mac Giolla Eain, Q. Xu, V. M. Egan, J. Punch, and A. M. Lyons, "Design and fabrication of a hybrid superhydrophobic–hydrophilic surface that exhibits stable dropwise condensation," ACS Appl. Mater. Interfaces **7**, 23575–23588 (2015).
[13]M. M. Garimella, S. Koppu, S. S. Kadlaskar, V. Pillutla, W. Choi *et al.*, "Difference in growth and coalescing patterns of droplets on bi-philic surfaces with varying spatial distribution," J. Colloid Interface Sci. **505**, 1065–1073 (2017).
[14]W. Xu, Z. Lan, B. L. Peng, R. F. Wen, and X. H. Ma, "Effect of surface free energies on the heterogeneous nucleation of water droplet: A molecular dynamics simulation approach," J. Chem. Phys. **142**, 054701 (2015).
[15]E. Da Riva and D. Del Col, "Numerical simulation of laminar liquid film condensation in a horizontal circular minichannel," J. Heat Transfer **134**, 051019 (2012).
[16]H. Ganapathy, A. Shooshtari, K. Choo, S. Dessiatoun, M. Alshehhi, and M. Ohadi, "Volume of fluid-based numerical modeling of condensation heat transfer and fluid flow characteristics in microchannels," Int. J. Heat Mass Transfer **65**, 62–72 (2013).
[17]H. Farhat, S. Kondaraju, S.-K. Na, and J. S. Lee, "Effect of hydrodynamic and fluid-solid interaction forces on the shape and stability of a droplet sedimenting on a horizontal wall," Phys. Rev. E **88**, 013013 (2013).
[18]A. Yagub, H. Farhat, S. Kondaraju, and T. Singh, "A lattice Boltzmann model for substrates with regularly structured surface roughness," J. Comput. Phys. **301**, 402–414 (2015).
[19]A. Budaraju, J. Phirani, S. Kondaraju, and S. S. Bahga, "Capillary displacement of viscous liquids in geometries with axial variations," Langmuir **32**, 10513–10521 (2016).
[20]Q. Li, K. H. Luo, Q. J. Kang, Y. L. He, Q. Chen, and Q. Liu, "Lattice Boltzmann methods for multiphase flow and phase-change heat transfer," Prog. Energy Combust. Sci. **52**, 62–105 (2016).
[21]A. K. Gunstensen, D. H. Rothman, S. Zaleski, and G. Zanetti, "Lattice Boltzmann model of immiscible fluids," Phys. Rev. A **43**, 4320–4327 (1991).
[22]X. Shan and H. Chen, "Lattice Boltzmann model for simulating flows with multiple phases and components," Phys. Rev. E **47**, 1815–1819 (1993).
[23]M. R. Swift, W. R. Osborn, and J. M. Yeomans, "Lattice Boltzmann simulation of nonideal fluids," Phys. Rev. Lett. **75**, 830–833 (1995).
[24]X. Shan and H. Chen, "Simulation of nonideal gases and liquid-gas phase transitions by the lattice Boltzmann equation," Phys. Rev. E **49**, 2941–2948 (1994).
[25]R. Zhang and H. Chen, "Lattice Boltzmann method for simulations of liquid-vapor thermal flows," Phys. Rev. E **67**, 066711 (2003).
[26]G. Házi and A. Márkus, "Modeling heat transfer in supercritical fluid using the lattice Boltzmann method," Phys. Rev. E **77**, 026305 (2008).
[27]Q. Li, Q. J. Kang, M. M. Francois, Y. L. He, and K. H. Luo, "Lattice Boltzmann modeling of boiling heat transfer: The boiling curve and the effects of wettability," Int. J. Heat Mass Transfer **85**, 787–796 (2015).
[28]G. Hazi and A. Markus, "On the bubble departure diameter and release frequency based on numerical simulation results," Int. J. Heat Mass Transfer **52**, 1472–1480 (2009).
[29]S. Gong and P. Cheng, "A lattice Boltzmann method for simulation of liquid–vapor phase-change heat transfer," Int. J. Heat Mass Transfer **55**, 4923–4927 (2012).
[30]Y. Vasyliv, D. Lee, T. Tower, R. Ng, V. Polashock, and A. Alexeev, "Modeling condensation on structured surfaces using lattice Boltzmann method," Int. J. Heat Mass Transfer **136**, 196–212 (2019).
[31]M. Li, C. Huber, W. Tao, and J. Wei, "Study on nucleation position and wetting state for dropwise condensation on rough structures with different wettability using multiphase lattice Boltzmann method," Int. J. Heat Mass Transfer **131**, 96–100 (2019).
[32]R. Haghani-Hassan-Abadi and M. H. Rahimian, "A lattice Boltzmann method for simulation of condensation on liquid-impregnated surfaces," Int. Commun. Heat Mass Transfer **103**, 7–16 (2019).
[33]N. D. Pawar, S. R. Kale, S. S. Bahga, H. Farhat, and S. Kondaraju, "Study of microdroplet growth on homogeneous and patterned surfaces using lattice Boltzmann modeling," J. Heat Transfer **141**, 062406 (2019).
[34]P. L. Bhatnagar, E. P. Gross, and M. Krook, "A model for collision processes in gases. I. Small amplitude processes in charged and neutral one-component systems," Phys. Rev. **94**, 511–525 (1954).
[35]D. Yu, R. Mei, L.-S. Luo, and W. Shyy, "Viscous flow computations with the method of lattice Boltzmann equation," Prog. Aerosp. Sci. **39**, 329–367 (2003).
[36]A. L. Kupershtokh and D. A. Medvedev, "Lattice Boltzmann equation method in electrohydrodynamic problems," J. Electrost. **64**, 581–585 (2006).
[37]A. L. Kupershtokh, D. A. Medvedev, and D. I. Karpov, "On equations of state in a lattice Boltzmann method," Comput. Math. Appl. **58**, 965–974 (2009), Mesoscopic Methods in Engineering and Science.
[38]P. Yuan and L. Schaefer, "Equations of state in a lattice Boltzmann model," Phys. Fluids **18**, 042101 (2006).
[39]P. K. Jain, A. Tentner, and Rizwan-uddin, "A lattice Boltzmann framework to simulate boiling water reactor core hydrodynamics," Comput. Math. Appl. **58**, 975–986 (2009).
[40]A. D. Angelopoulos, V. N. Paunov, V. N. Burganos, and A. C. Payatakes, "Lattice Boltzmann simulation of nonideal vapor-liquid flow in porous media," Phys. Rev. E **57**, 3237–3245 (1998).
[41]N. D. Pawar, S. S. Bahga, S. R. Kale, and S. Kondaraju, "Symmetric and asymmetric coalescence of droplets on a solid surface in the inertia-dominated regime," Phys. Fluids **31**, 092106 (2019).
[42]K. K. Varanasi, M. Hsu, N. Bhate, W. Yang, and T. Deng, "Spatial control in the heterogeneous nucleation of water," Appl. Phys. Lett. **95**, 094101 (2009).